

Interpreting Black-box Machine Learning Models for High Dimensional Datasets

Md. Rezaul Karim^{*†}, Md Shajalal^{†‡}, Alexander Graß^{†*}, Till Döhmen[†], Sisay Adugna Chala^{†*},
Alexander Boden^{†¶}, Christian Becks^{§†}, and Stefan Decker^{*†}

^{*} Computer Science 5 - Information Systems and Databases, RWTH Aachen University, Germany

[†] Fraunhofer - Institute for Applied Information Technology FIT, Germany

[‡] University of Siegen, Germany

[§] University of Hagen, Germany

[¶] Bonn-Rhein-Sieg University of Applied Sciences, Germany

Abstract—Many datasets are of increasingly high dimensionality, where a large number of features could be irrelevant to the learning task. The inclusion of such features would not only introduce unwanted noise but also increase computational complexity. Deep neural networks (DNNs) outperform machine learning (ML) algorithms in a variety of applications due to their effectiveness in modelling complex problems and handling high-dimensional datasets. However, due to non-linearity and higher-order feature interactions, DNN models are unavoidably opaque, making them *black-box* methods. In contrast, an interpretable model can identify statistically significant features and explain the way they affect the model’s outcome. In this paper[†], we propose a novel method to improve the interpretability of black-box models in the case of high-dimensional datasets. First, a black-box model is trained on full feature space that learns useful embeddings on which the classification is performed. To decompose the inner principles of the black-box and to identify top-k important features (global explainability), probing and perturbing techniques are applied. An interpretable *surrogate model* is then trained on top-k feature space to approximate the black-box. Finally, decision rules and counterfactuals are derived from the surrogate to provide local decisions. Our approach outperforms tabular learners, e.g., TabNet and XGboost, and SHAP-based interpretability techniques, when tested on a number of datasets having dimensionality between 54 and 20,531².

Index Terms—Curse of dimensionality, Black-box models, Interpretability, Attention mechanism, Model surrogation.

I. INTRODUCTION

High availability and easy access to large datasets, AI accelerators, and state-of-the-art machine learning (ML) and deep learning (DNNs) algorithms paved the way for performing predictive modelling at scale. However, in the case of high-dimensional datasets (e.g., omics), the feature space exponentially increases. Principal component analysis (PCA) and isometric feature mapping (Isomap) are widely used to tackle the curse of dimensionality [1]. Although they preserve inter-point distances, they are fundamentally limited to linear embedding and tend to lose useful information, which makes them less effective in dimensionality reduction [2]. The inclusion of a large number of irrelevant features not

only introduces unwanted noise but also increases computational complexity as the data becomes sparser. With increased modelling complexity involving hundreds of features and their interactions, making a general conclusion or interpreting the black-box model’s outcome becomes increasingly difficult, whereas many approaches do not take into account understanding the inner structure of opaque models.

In contrast, DNNs benefit from higher pattern recognition capabilities during learning useful representation from such datasets. With multiple hidden layers and non-linear activation functions within layers, autoencoder (AEs) can model complex and higher-order feature interactions. Learning non-linear mappings allow embedding input feature space into a lower-dimensional latent space. Such representations can be used for both supervised and unsupervised downstream tasks [3]. The embedding can capture contextual information of the data [3]. However, predictions from such a *black-box* model can neither be traced back to the input, nor it is clear why outputs are transformed in a certain way. This exposes even the most accurate model’s inability to answer questions like “*how and why inputs are ultimately mapped to certain decisions*”. In sensitive areas like banking and healthcare, explainability and accountability are not only some desirable properties of AI but also legal requirements – especially where AI would have a significant impact on human lives [4]. Therefore, legal landscapes are fast-moving in European and North American countries, e.g., *EU GDPR* enforces that processing based on automated decision-making tools should be subject to suitable safeguards, including “*right to obtain an explanation of the decision reached after such assessment and to challenge the decision*”. Since how decisions are made should be as transparent as possible in a faithful and interpretable manner.

Explainable AI (XAI), which gains a lot of attention from both academia and industries, aims to overcome the opaqueness of black-boxes and brings transparency in AI systems. Model-specific and model-agnostic approaches covering local and global interpretability have emerged [5]. While local explanations focus on explaining individual predictions, global explanations explain entire model behaviour using plots or decision sets. Although an interpretable model can explain how it makes a prediction by exposing important factors that

¹ This paper is accepted and included in proceedings of 2023 IEEE 10th International Conference on Data Science and Advanced Analytics (DSAA’2023) ² GitHub: <https://github.com/rezacsedu/DeepExplainHidim>

influence its outcomes, interpretability comes at the cost of efficiency. Research suggested by learning an interpretable model to approximate a black-box globally in order to provide local explanations [6]. A surrogate model’s input-output behaviour can be represented in a more human-interpretable using decision rules (DRs). DRs containing *antecedents* (IF) and a *consequent* (THEN) provide intuitive explanations³ than graph- or plot-based explications [6].

Further, humans tend to think in a counterfactual way by asking questions like “How would the prediction have been if input x had been different?”⁴. By using a set of rules and counterfactuals, it is possible to explain decisions directly to humans with the ability to comprehend the underlying reason so that users can focus on⁵ learned knowledge without emphasising underlying data representations. Keeping in mind the practical and legal consequences of using black-box models, we propose a novel method to improve the interpretability of black-box models for classification tasks. We hypothesize that: i) by decomposing the inner logic (e.g., most important features), the opaqueness of a black-box can be mitigated by outlining the most (e.g., *top-k feature space*) and least important features, ii) by finding a sub-domain of full feature space, would allow us training a surrogate model, which will sufficiently be able to approximate the black-box model, and ii) a representative decision rule set can be generated with the surrogate, which can be used to sufficiently explain individual decisions in a human-interpretable way.

II. RELATED WORK

Existing interpretable ML methods can be categorized as either model-specific or model-agnostic with a focus on local and global interpretability or either. Local interpretable model-agnostic explanations (LIME) [7], model understanding through subspace explanations (MUSE) [8], SHapley Additive exPlanations (SHAP) [9], partial dependence plots (PDP), individual conditional expectation (ICE), permutation feature importance (PFI), counterfactual explanations (CE) [5] are among others. These methods operate by approximating the outputs of an opaque model via tractable logic, such as game theoretic Shapley values (SVs) or local approximation of complex or black-box models via a linear model [10]. Since these approaches do not take into account the inner structure of an opaque black-box model, probing, perturbing, attention mechanism, sensitivity analysis (SA), saliency maps, and gradient-based attribution methods have been proposed to understand the underlying logic of complex models.

Saliency map and gradient-based methods can identify relevant regions and assign importance to each feature, e.g., image pixels, where first-order gradient information of a

³ An example rule for a loan application denial could be “IF monthly_income = 3000 AND credit_rating_history=BAD AND employment_status=YES AND married=YES, THEN decision = DENY” ⁴ “What would have been the decision if my monthly income would be higher?” ⁵ “Although you’re employed, given your monthly income of 2,000 EUR and having bad credit rating history, our model has denied your application, as we think you’re unlikely to repay. Even though you have had bad credit rating history, an increase in your monthly income of 1,000 EUR will definitely end up with acceptance, as you’re already employed.”

black-box model is used to produce heatmaps indicating their relative importance. Gradient-weighted class activation mapping (Grad-CAM++) [11] and layer-wise relevance propagation (LRP) [12] are examples of this category that highlight relevant parts of inputs, e.g., images to a DNN which caused the decision can be highlighted. Attention mechanisms are used in a variety of supervised and language modelling tasks, as they can detect larger subsets of features. Self-attention network (SAN) [13] is proposed to identify important features from tabular data. TabNet [14] uses sequential attention to choose a subset of semantically meaningful features to process at each decision step. It also visualizes the importance of features and how they are combined to quantify the contribution of each feature to the model enabling local and global interpretability. SAN is found effective on datasets having a large number of features, while its performance degrades in the case of smaller datasets, indicating that having not enough data can distil the relevant parts of the feature space [13]. Model interpretation strategies are proposed that involve training an inherently interpretable *surrogate* model to learn a locally faithful approximation of a black-box model [6]. Since an explanation relates the feature values of a sample to its prediction, rule-based explanations are easier to understand for humans. Anchor [15] is a rule-based method that extends LIME, which provides explanations in the form of decision rules. Anchor computes rules by incrementally adding equality conditions in the antecedents, while an estimate of the rule precision is above a threshold [16].

A drawback of rule-based explanations is overlapping and contradictory rules. Sequential covering (SC) and Bayesian rule lists (BRL) are proposed to deal with these. SC iteratively learns a single rule covering the entire training data rule-by-rule and removes the data points that are already covered by new rules, while SBRL combines pre-mined frequent patterns into a decision list using Bayesian statistics [6]. *Local rule-based explanations* (LORE) [16] is proposed to overcome these issues. LORE learns an interpretable model of a neighbourhood based on genetic algorithms. LORE derives explanations via the interpretable model and provides local explanations in the form of a *decision rule* and *counterfactuals* - that signifies making what feature values may lead to a different outcome. LIME indicates where to look for a decision based on feature values, while counterfactual rules of *LORE* signify minimal-change contexts for reversing the predictions.

III. METHODS

Each high-dimensional dataset has a large feature space. Therefore, first, we train a black-box model to learn representations. Then, we classify the data points on their embedding space instead of the original feature space. To decompose the inner structure of the black box, probing and perturbing techniques are applied to identify *top-k* features that contribute most to the overall model’s decision-making. An interpretable surrogate model is then built on top-k features to approximate the black-box. Finally, *decision-rules* and *counterfactuals* are generated from the surrogate to explain individual decisions.

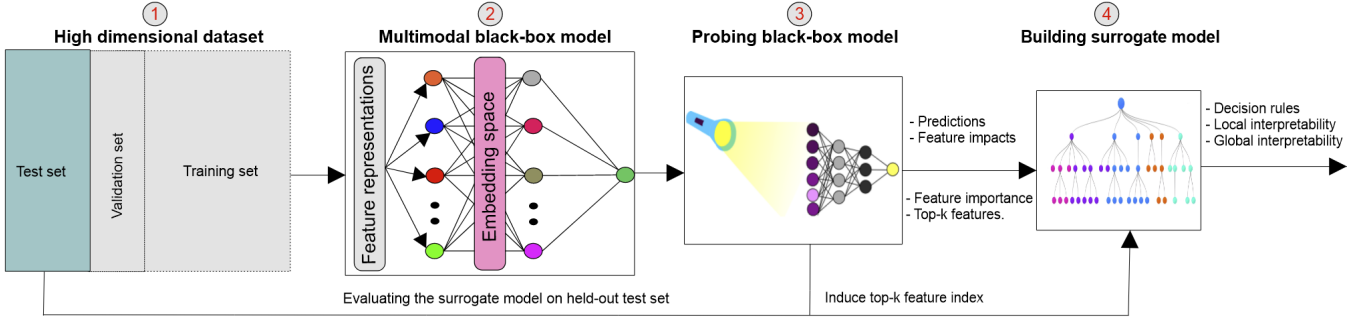


Fig. 1: Workflow of our proposed approach (recreated based on Karim et al. [17])

A. Building black-box models

Figure 1 shows the workflow of our proposed approach for interpreting black-box models. Input X is first fed into a DNN to generate latent representations. It embeds the feature space into a lower dimensional latent space, s.t. X is transformed with a nonlinear mapping $f_\Theta : X \rightarrow Z$, where $Z \in \mathbb{R}^K$ are learned embeddings, where $K \ll F$. A fully-connected *softmax* layer is added on top of DNN by forming a black-box classifier f_b . To parameterize f_b , we train a convolutional autoencoder (CAE). The function approximation properties and feature learning capabilities help CAE extract deep and quality features [3]. Further, since weights are shared among layers, CAEs have the locality-preserving capability and can reduce the number of parameters compared to other AEs.

A convolutional layer calculates feature maps (FMs) that are passed through max-pooling to downsample by taking the maximums in each non-overlapping sub-region, which maps input X into a lower-dimensional embedding space Z [3]:

$$Z = g_\phi(X) = \sigma(W \otimes X + b), \quad (1)$$

where encoder $g(\cdot)$ is a *sigmoid* function parameterized by $\phi \in \Theta$ that include a weight matrix $W \in \mathbb{R}^{p \times q}$ and a bias vector $b \in \mathbb{R}^q$ in which p and q are numbers of input and hidden units, \otimes is the convolutional operation, Z are the latent variables, and σ is the exponential linear unit activation function. The decoder $h(\cdot)$ reconstructs the input X from latent representation Z by applying unpooling and deconvolution s.t. Z is mapped back to a reconstructed version $X' \approx X$ as [3]:

$$X' = h_\Theta(Z) = h_\Theta(g_\phi(X)), \quad (2)$$

where $h(\cdot)$ is parameterized by $(\theta, \phi) \in \Theta$ that are jointly learned to generate X' . This is learning an identity function, i.e., $X' \approx h_\theta(g_\phi(X))$. Mean squared error (MSE) measures the reconstruction loss L_r :

$$L_r(\theta, \phi) = \frac{1}{N} \sum_{i=1}^N (X - X')^2 + \lambda \|W\|_2^2 \quad (3)$$

where λ is the activity regularizer and W is a vector containing network weights. Therefore, $h_\theta(g_\phi(X))$ is equivalent

to $\Psi(W' * Z + b')$ [3], which makes $X' = \Psi(W' \odot Z + b')$, where \odot is the transposed convolution operation, W' is decoder's weights, b' is bias vectors, and Ψ is the sigmoid activation function. The unspooling is performed with switch variables [18] to remember the positions of the maximum values during the max-pooling operation. Within each neighbourhood of Z , both value and location of maximum elements are recorded: pooled maps store values, while switches record the locations. Z is fed into a fully-connected *softmax* layer for the classification, which maps a latent point z_i into an output $f_b(z_i) \mapsto \hat{y}_i$ in the embedding space Z by optimizing categorical cross-entropy (CE) loss (binary CE in the case of binary classification) during back-propagation. Reconstruction- and CE loss of CAE are then combined and optimized jointly [3]:

$$L_{cae} = \sum_{i=1}^n \alpha_r L_r + \alpha_{ce} L_{ce}, \quad (4)$$

where α_r and α_{ce} are the regularization weights for reconstruction and CE loss functions, respectively.

B. Interpreting black-box models

We apply probing, perturbing and model surrogation techniques to interpret the black-box model.

1) *Probing with attention mechanism*: The SAN_{CAE} architecture, which in fig. 2 enables self-attention at the feature level. An attention layer is represented as [13]:

$$l_2 = \sigma(W_2 \cdot (\alpha(W_{|F|} \cdot \Omega(X) + b_{l_1})) + b_{l_2}), \quad (5)$$

where α is an activation function, b_{l_i} is layer-wise bias, and Ω is the following first network layer that maintains the connection with input features X [13]:

$$\Omega(X) = \frac{1}{k} \bigoplus_k [X \otimes \text{softmax}(W_{l_{att}}^k X + b_{l_{att}}^k)] \quad (6)$$

where X is first used as input to a softmax-activated layer by setting the number of neurons to $|F|$, k is the number of attention heads representing relations between input features, and $W_{l_{att}}^k$ is a set of weights in respective attention heads. On the other hand, the *softmax* function, which is applied to i -th element of a weight vector v is defined as follows [13]:

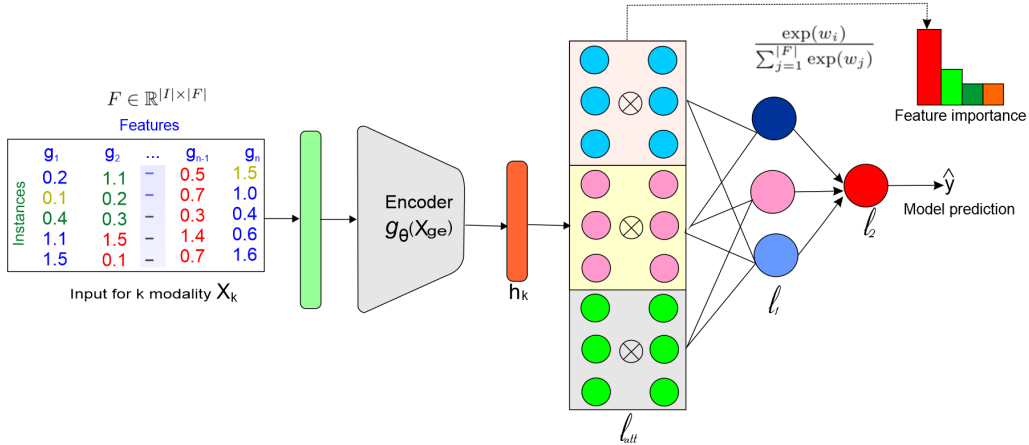


Fig. 2: Schematic representation of SAN_{CAE} model (recreated based on Karim et al. [17])

$$\text{softmax}(v_i) = \frac{\exp(v_i)}{\sum_{i=1}^{|F|} \exp(v_i)} \quad (7)$$

where $W_{l_{att}}^k \in \mathbb{R}^{|F| \times |F|}$, $v \in \mathbb{R}^{|F|}$, and l_{att} represents the attention layer in which element-wise product with X is computed in forward pass to predict labels \hat{y} , where two consecutive dense layers l_1 and l_2 contribute to predictions, \otimes and \oplus are Hadamard product- and summation across k heads. As Ω maintains a bijection between features and attention head's weights, weights in $|F| \times |F|$ matrix represent relations between features. We hypothesize that a global weight vector can be generated by applying attention to the encoder's bottleneck layer. The vector is used to compute feature attributions. Unlike SAN, we apply attention to embedding space (encoder's deepest conv. layer) that can be defined as follows that maintains connections between latent features Z [13]:

$$\Omega(Z) = \frac{1}{k} \bigoplus_k [Z \otimes \text{softmax}(W_{l_{att}}^k Z + b_{l_{att}}^k)]. \quad (8)$$

Embedding Z is used as the input to the *softmax* layer in which the number of neurons is equal to the dimension of embedding space. *Softmax* function applied to i -th element of weight vector v_z as follows [13]:

$$\text{softmax}(v_{z_i}) = \frac{\exp(v_{z_i})}{\sum_{i=1}^{|Z|} \exp(v_{z_i})}; v_{z_i} \in \mathbb{R}^{|Z|} \quad (9)$$

Once the training is finished, the attention layer's weights are activated using softmax as follows [19]:

$$R_l = \frac{1}{k} \bigoplus_k [\text{softmax}(\text{diag}(W_{l_{att}}^k))], \quad (10)$$

where $W_{l_{att}}^k \in \mathbb{R}^{|Z| \times |Z|}$. As the surrogate is used to provide local explanations, top- k features are extracted as diagonal of $W_{l_{att}}^k$ and ranked w.r.t. their weights.

2) *Perturbing with sensitivity analysis*: We validate globally important features through SA. We change a feature value by keeping other features unchanged. If any change in its value significantly impacts the prediction, the feature is considered to have a high impact on the prediction. We create a new set \hat{X}^* by applying w -perturbation over feature a_i and measure its sensitivity at the global level. To measure the change in predictions, we observe MSE between actual and predicted labels and compare the probability distributions over the classes⁶. Sensitivity S of a feature a_i is the difference between MSE at original feature space X and sampled \hat{X}^* . However, since SA requires a large number of calculations⁷, we make minimal changes to top- k features only in order to reduce the computational complexity.

3) *Model surrogation*: Model surrogation is a knowledge distillation process by finding a sub-domain of feature space, thereby approximating the teacher via student, under the constraint that the student is interpretable. Since most important features are already identified by the black-box f_b , we hypothesize that training a surrogate f on top- k feature space would be sufficient. As described in algorithm 1, we train f on sampled data X^* ⁸ and ground truths Y .

Since any interpretable model can be used for the function g [6], we train decision tree (DT), random forest (RF), and XGBoost classifiers⁹ classifiers. DT iteratively splits X^* into multiple subsets w.r.t to threshold values of features at each node until a leaf node containing decision is reached. The mean importance of a feature a_i is computed by going through all splits for which a_i was used and adding up how much it has improved the prediction in a child node Q w.r.t Gini $I_{GQ} = \sum_{k=1}^N p_k \cdot (1 - p_k)$, where p_k is the number of instances having label y_k^* in Q . RF and XGBoost ensemble randomized predictions to get the final decisions.

⁶ Two most probable classes in multi-class settings. ⁷ e.g., $N \times M$; N and M are the number of instances and features. ⁸ A sub-feature-space containing important features only. ⁹ Eventhough RF and XGBoost are complex tree ensembles and known to be black-boxes, DTs can be extracted from. The best DT estimator can be used for computing FI.

Algorithm 1: Black-box model surrogation

Input : A simplified version X^* of dataset D (e.g., top- k feature space identified by f_b), black-box model f_b , interpretable model type t , and model parameters Θ^* .

Output: A surrogate model f and its predictions \hat{Y}_{test}^* on held-out test set.

$X_{train}^*, Y_{train}^*, X_{test}^*, Y_{test}^* \leftarrow$
 $TrainTestSplit(X^*, Y)$

$X_{train}, Y_{train}, X_{test}, Y_{test} \leftarrow TrainTestSplit(X, Y)$

$clf \leftarrow Estimator(t, \Theta^*)$ // Create estimator

for all batches in train set $\in X_{train}^*$ **do**

$f \leftarrow clf.fit(X_{train}^*, Y_{train}^*)$ // Train surrogate

return f

end

$M \leftarrow [f, f_b]$ // List of models, where f_b is trained on X_{train}

for model $\in M$ **do**

 // Generate predictions

$\hat{Y}_{test} \leftarrow f_b.predict(X_{test})$ // for black-box

$\hat{Y}_{test}^* \leftarrow f.predict(X_{test}^*)$ // for surrogate

return $\{f_b, \hat{Y}\}, \{f, \hat{Y}_*\}$

end

C. Feature impacts and decision rules

We assume the black-box f_b has sufficient knowledge and the surrogate f has learned the mapping $Y^* = f(X^*)$. We hypothesize that f is able to mimic f_b . We compute permutation feature importance (PFI) for f as a view to global feature importance (GFI). However, since PFI does not necessarily reflect the intrinsic predictive value of a feature, features having lower importance for an under-/overfitted model could be important for a better-fitted model [20]. We use SHAP to generate more consistent explanations. SHAP importance for $a_i \in x$ is computed by comparing what f predicts with and without a_i for all possible combinations of $M-1$ features (i.e., except for a_i) w.r.t SV ϕ_i [20]. Since the order in which the features are observed by a model impacts its outcome, SVs explain the output of a function as the sum of effects ϕ_i of each feature being observed into a conditional expectation. If a_i has zero effect on the prediction, an SV of 0 is expected. If two features contribute equally, their SVs would be the same [9].

To compute GFI, absolute SVs per feature across all instances are averaged. Then, to generate consistent GFI, we create a stacking ensemble of SVs by averaging the marginal outputs from DT, XGBoost, and RF models. We derive decision rules from a root-leaf path in a DT: starting at the root

and satisfying the split condition of each decision node, we traverse until a leaf node is reached (fig. 1 in supplementary). Unlike in a DT, a decision can be reached through multiple rules with excessive lengths. Given the huge feature space, textual representations would obstruct human-interpretability especially when the rule list length is large. Therefore, to mitigate the issue of overlapping rules, we create an ordered list of inclusive rules based on SBRL.

Rules with low confidence are insignificant in discriminating classes and may not be useful in explaining the decisions. Therefore, we filter rules that do not meet coverage, support, and confidence. Besides, we restrict the antecedents to be a conjunction of clauses (i.e., condition on feature a_i). The output of each rule is a probability distribution¹⁰. Using SBRL, pre-mined frequent patterns are combined into a decision list R having representative rules. Finally, the faithfulness is computed w.r.t *coverage* that maximizes the fidelity of the rule list. Similar to Grath *et al.* [21], we generate counterfactuals by calculating the smallest possible changes (Δx) to input x s.t. the outcome flips from prediction y to y' .

IV. EXPERIMENTS

We evaluate our approach on a number of datasets for classification tasks. However, our approach is dataset-agnostic and can be applied to any tabular dataset. We implemented our methods in Python using *scikit-learn*, *Keras*, and *PyTorch*. To provide a fair comparison, we train TabNet and XGBoost classifiers as they are effective for tabular datasets. We train multilayer perceptron (MLP) on PCA projection space. We provide qualitative and quantitative evaluations of each model, covering local and global explanations. We report precision, recall, F1-score, and *Matthews correlation coefficient* (MCC) scores. We assess the quality of rules w.r.t support and fidelity. To assess how well f has replicated f_b , R-squared measure (R^2) is calculated as the percentage of the variance of the predictions from f_b captured by the surrogate itself and expressed as an indicator for goodness-of-fit [3]:

$$R^2 = 1 - \frac{SSE^*}{SSE} = 1 - \frac{\sum_{i=1}^N (\hat{y}_i^* - \hat{y}_i)^2}{\sum_{i=1}^N (\hat{y}_i - \hat{y})^2}, \quad (11)$$

where \hat{y}_i^* is the prediction for f , \hat{y}_i is the prediction for f_b for X^* , and SSE and SSE^* are the sum of square errors for f and f_b , respectively [6]. If f can be used instead of f_b :

- if R^2 is close to 1 (low error), the surrogate model approximates the behavior of the *black-box* model very well. Hence, the surrogate model f can be used instead of the black-box model f_b .
- if R^2 is close to 0 (high error), the surrogate fails to approximate the *black-box*, hence cannot replace f_b .

A. Datasets

We experimented on four datasets: i) gene expression from *Pan Cancer Atlas* project, having 20,531 features and covering 33 tumour types, ii) indoor localization (UJIndoorLoc) [22]

¹⁰ Probability an instance satisfies an antecedent to belong to a class.

TABLE I: Performance of individual models

Model	Dataset	Precision	Recall	F1	MCC
<i>MLP_{PCA}</i>	Gene expr.	0.7745	0.7637	0.7553	0.7367
	UJIndoorLoc	0.8652	0.8543	0.8437	0.7741
	Health advice	0.8743	0.8679	0.8564	0.8067
	Forest cover	0.7654	0.7547	0.7522	0.7126
<i>XGBoost</i>	Gene expr.	0.8725	0.8623	0.8532	0.7851
	UJIndoorLoc	0.8964	0.8931	0.8836	0.7959
	Health advice	0.9354	0.9301	0.9155	0.8211
	Forest cover	0.8382	0.8265	0.8184	0.7963
TabNet	Gene expr.	0.9326	0.9276	0.9175	0.8221
	UJIndoorLoc	0.9217	0.9105	0.9072	0.8051
	Health advice	0.9455	0.9317	0.9178	0.8235
	Forest cover	0.8953	0.8879	0.8854	0.8057
<i>SAN_{CAE}</i>	Gene expr.	0.9525	0.9442	0.9325	0.8353
	UJIndoorLoc	0.9357	0.9269	0.9175	0.8233
	Health advice	0.9623	0.9538	0.9329	0.8451
	Forest cover	0.9112	0.9105	0.9023	0.8124

having 523 variables, iii) *health advice* having 123 variables¹¹, and ii) *forest cover type* dataset [23] having 54 variables.

B. Model performance analyses

We report the performance of each model w.r.t. increasing latent dimensions in fig. 3. When the dimension increases, accuracy also increases and the inter-model difference reduces, until a certain point where accuracy decreases again. In the case of lower dimensional datasets (e.g., *health advice* and *forest cover*), accuracy improves up to $45 \approx 55\%$ of projected dimension. However, embedding them into much lower dimensions loses useful information to correctly classify data points, yielding significant accuracy drop. In the case of higher dimensional datasets (e.g., GE, UJIndoorLoc), more dimensions bring more noise than information, which makes the classification harder (a model is no better than baseline, e.g., 5% for GE and 9% for UJIndoorLoc). Projecting them into $5 \approx 7\%$ embedding dimension unlikely to lose information.

MLP_{PCA} asymptotically yields the lowest accuracy across datasets (table I), while *XGBoost_{Isomap}* slightly outperformed *MLP_{PCA}*. As PCA features are projected onto an orthogonal basis, they are linearly uncorrelated. PCA is similar to a single-layered AE with a linear activation. Isomap learns a projection that preserves the intrinsic structure, but it fails to learn complex mappings. *SAN_{CAE}* and *TabNet* yielded comparable accuracy as both models learn projections that preserve relevant information for the classification. However, *SAN_{CAE}* outperformed *TabNet* as CAE modelled non-linear interactions among a large number of features and generate classification-friendly representations. We investigate the precision plot and lift curve in fig. 6 and fig. 7: while the former outlines the relation between predicted probability (that an index belongs to positive) and the percentage of an observed index in the positive class¹², the latter shows the percentage of positive classes when observations with a score above the cutoff are selected vs. random selection. Besides, we observe the decision boundary (DB)¹³ in fig. 5. Each model classifies

¹¹ <https://github.com/itachi9604/healthcare-chatbot> ¹² The observations get binned together in groups of roughly equal predicted probabilities and the percentage of positives is calculated for each bin. ¹³ Decision boundary is a hyper-surface that partitions the feature space.

data points¹⁴ on one side of the DB as belonging to one class and all those on the other side as belonging to another class.

C. Performance of surrogate models

The fidelity and confidence of the rule set on test sets are demonstrated in table II. The mean fidelity is shown in percentage and the standard deviations (SDs) for 5 runs are reported as \pm . Fidelity levels of 80%, 60% to 80%, and below 60% are considered high, medium, and low, respectively.

As of *UJIndoorLoc*, the XGBoost model achieved the highest fidelity and confidence scores of 90.25% and 89.15%, with SDs of 1.38% and 1.57%. RF model performed moderately well giving the second highest scores of 88.11% and 90.25%, with SDs of 1.21% and 1.38%. As of *health advice*, XGBoost achieved the highest fidelity and confidence of 91.38% and 90.25%, with SDs of 1.65% and 1.42%, respectively. RF model also performed moderately well giving the second highest fidelity and confidence of 90.11% and 89.45%, with slightly lower SDs of 1.81% and 1.35%.

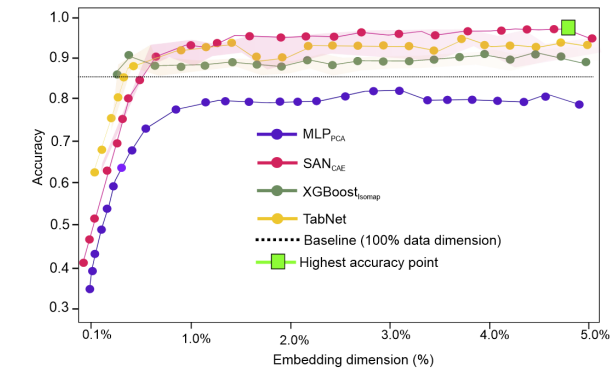
As of *forest cover type*, the XGBoost model achieved the highest fidelity and confidence of 94.36% and 92.17%, with the SDs of 1.35% and 1.34%. RF model performing moderately well too, yielding the second highest fidelity and confidence of 93.15% and 91.25%, with slightly lower SDs of 1.42% and 1.31%. As of *gene expression*, XGBoost model achieved highest fidelity and confidence of 93.45% and 91.37%, with the SDs of 1.25% and 1.35%. RF model also performed moderately well giving second highest scores of 92.25% and 90.21%, with slightly lower SDs of 1.35% and 1.29%. The R^2 for surrogates are reported in table III. The R^2 for the XGBoost model is comparable to the best performing *SAN_{CAE}* as well as the *TabNet* model.

D. Global interpretability

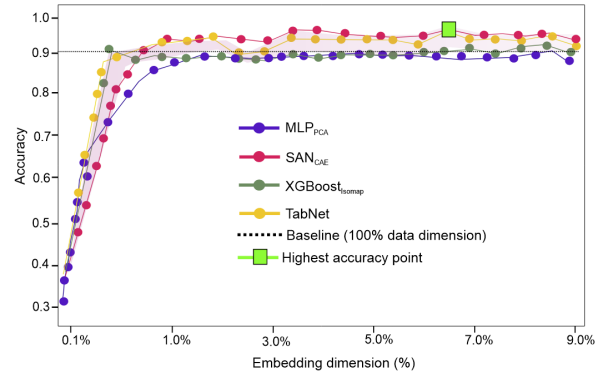
Accurate identification of the most and least significant features helps understand their relevance w.r.t certain classes. For example, biologically relevant genes provide insights into carcinogenesis as they could be viewed as potential biomarkers for specific cancer types. However, providing global and local explanations for all datasets will be overwhelming, so we focus on the gene expression dataset. Therefore, both GFI and impacts are analysed to understand the model's behaviour. Common and important features (w.r.t GFI) identified with *SAN_{CAE}* are identified, where GFI assign a score to input features based on how useful they are at predicting a target class or overall classes. However, unlike feature impact, feature importance does not provide which features in a dataset have the greatest positive or negative effect on the outcomes.

Therefore, global feature impacts sorted from most to least important of SHAP value, are shown in fig. 4, for model *SAN_{CAE}*. SHAP gives slightly different views on feature impacts: SPRR1B, ADCY3, FAM50B, SEMA3E, SLN, HAGLROS, CXCL10, VPS9D1-AS1, TRIM17, CLTRN, APLP1, and CWH43 positively impact the prediction. It signifies if the prediction is in favour of a cancer type (e.g.,

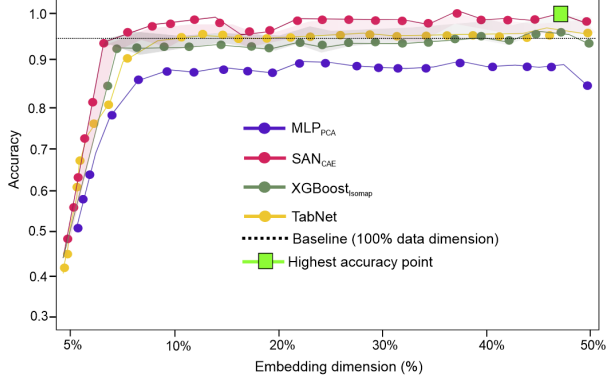
¹⁴ Shown 5 classes only as covering all 33 classes is overwhelming.



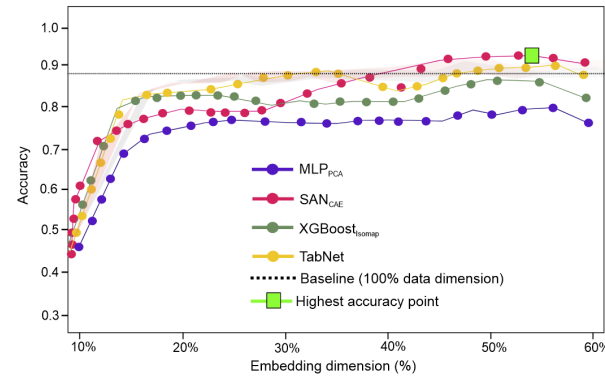
(a) Gene expression



(b) Indoor localization

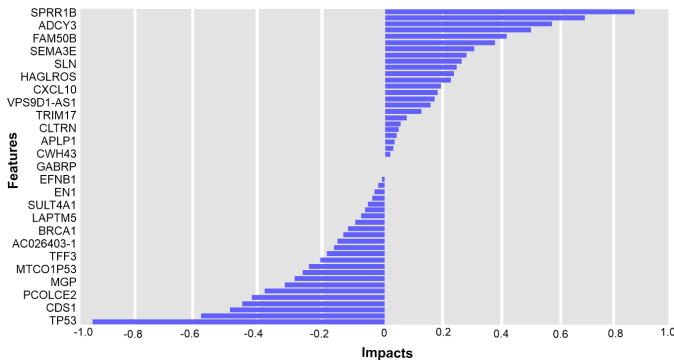


(c) Health advice

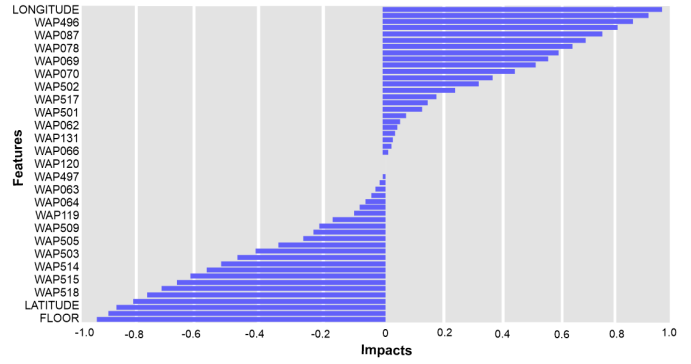


(d) Forest cover type

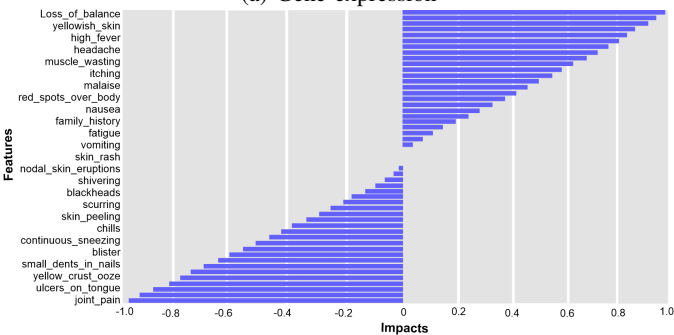
Fig. 3: Mean accuracy w.r.t relative dimension of latent space across datasets. Shade indicates standard deviation. The baseline is obtained by training the *TabNet* model on original feature space (i.e., 100% of the dimensions)



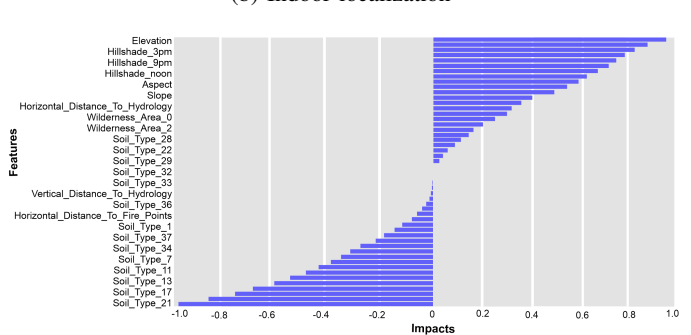
(a) Gene expression



(b) Indoor localization



(c) Health advice



(d) Forest cover type

Fig. 4: Global feature impacts sorted in terms of global feature impacts

TABLE II: Fidelity vs. confidence of rule sets for the surrogate models

Dataset	DT		RF		XGBoost	
	Fidelity	Confidence	Fidelity	Confidence	Fidelity	Confidence
UJIndoorLoc	86.16 ± 1.72	85.37 ± 1.53	89.27 ± 1.46	88.11 ± 1.21	90.25 ± 1.38	89.15 ± 1.57
Health advice	88.35 ± 1.45	87.55 ± 1.85	90.11 ± 1.81	89.45 ± 1.35	91.38 ± 1.65	90.25 ± 1.42
Forest cover type	90.23 ± 1.37	88.75 ± 1.32	93.15 ± 1.42	91.25 ± 1.31	94.36 ± 1.35	92.17 ± 1.34
Gene expression	91.27 ± 1.42	89.33 ± 1.25	92.25 ± 1.35	90.21 ± 1.29	93.45 ± 1.25	91.37 ± 1.35

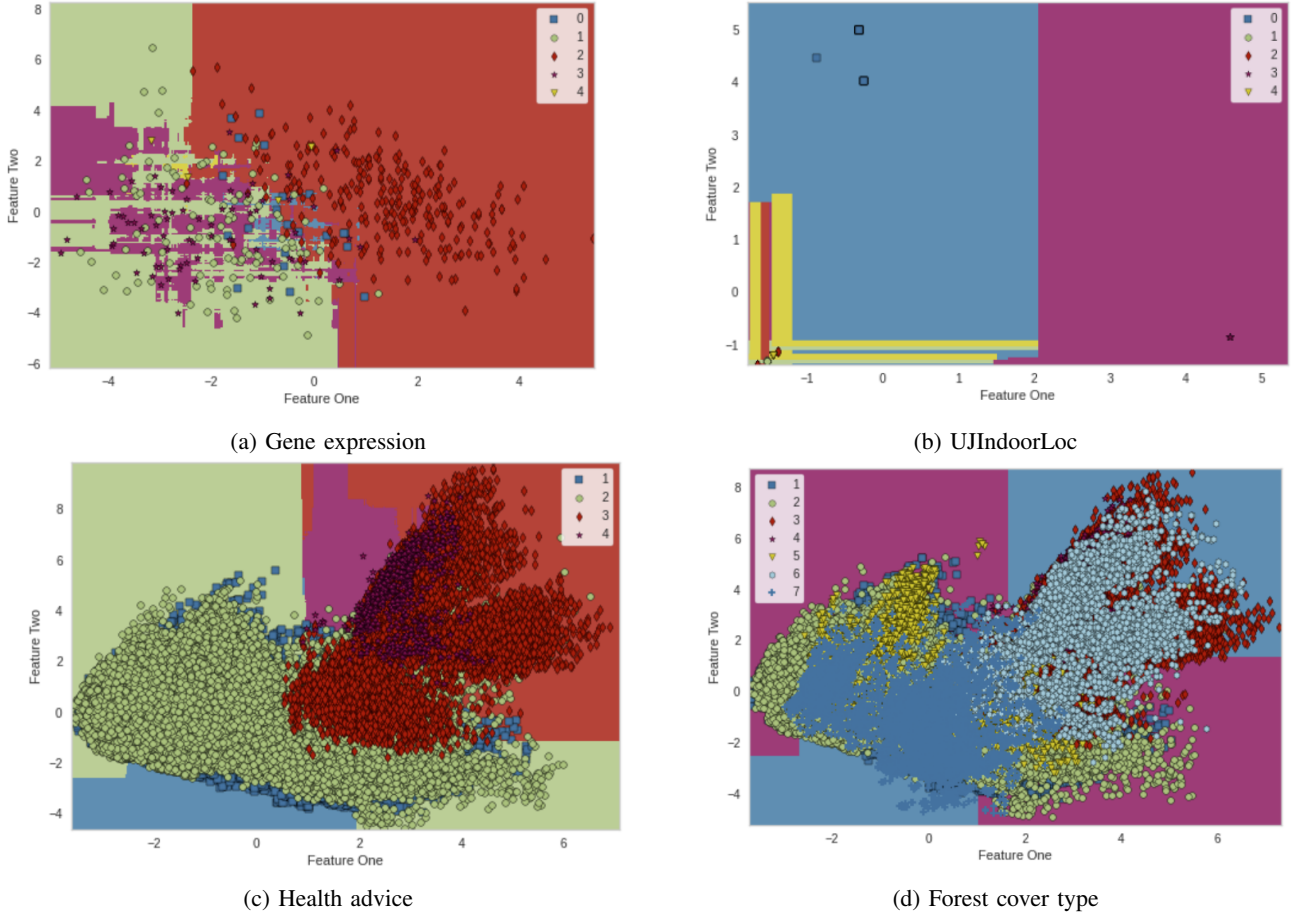


Fig. 5: Decision boundaries for XGboost model across datasets for top-2 features

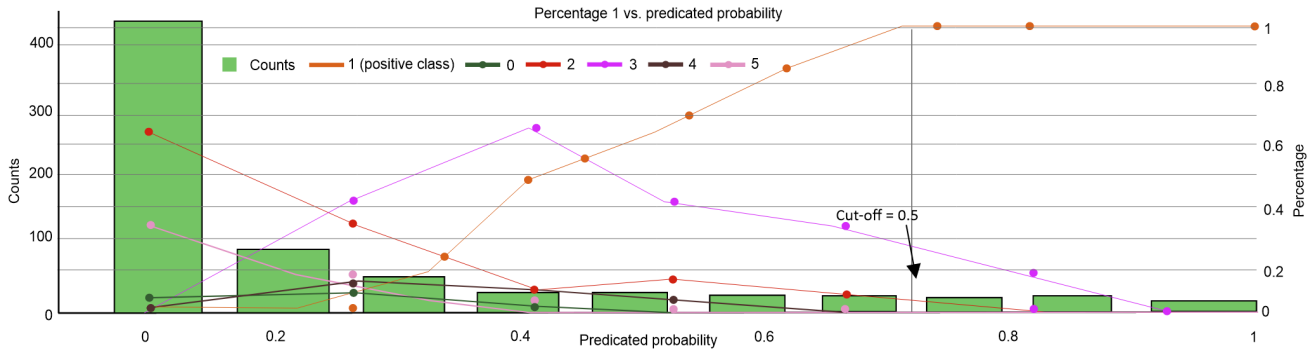


Fig. 6: Precision plot for the SAN_{CAE} model trained on GE dataset

COAD), these variables will play a crucial role in maintaining this prediction. Conversely, *TP53*, *CDS1*, *PCOLCE2*, *MGP*, *MTCO1P53*, *TFF3*, *AC026403-1*, *BRCA1*, *LAPTM5*,

SULT4A1, *EN1*, *EFNB1*, and *GABRP* have negative impacts on the prediction. It means if the prediction is *COAD* and the value of these variables are increased, the final prediction is

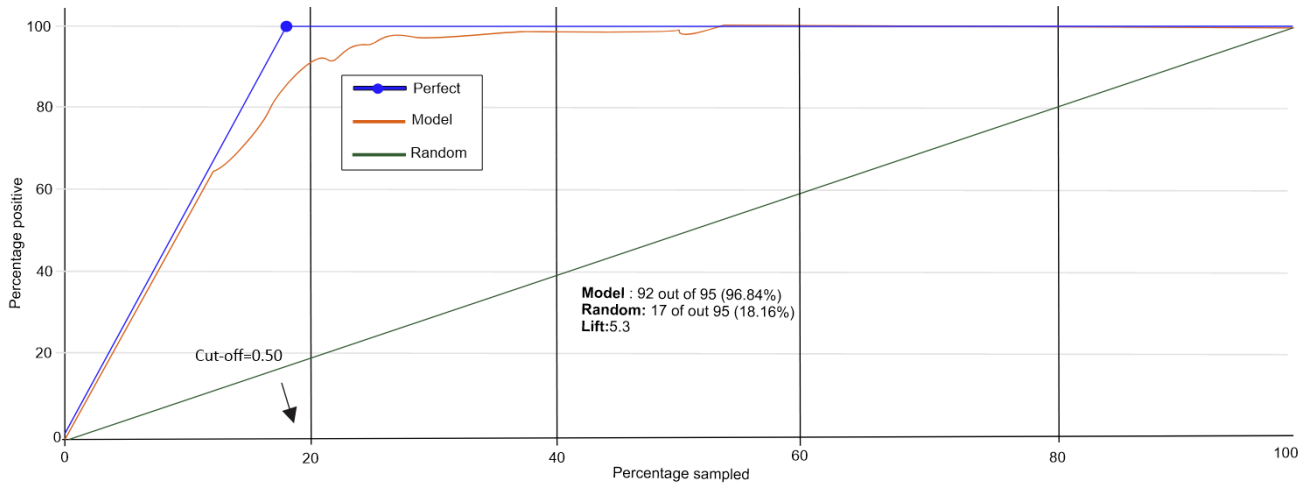


Fig. 7: Lift curve for the SAN_{CAE} model trained on GE dataset

TABLE III: Percentage of variance (R^2) of surrogates

Dataset	DT	RF	XGBoost
UJIndoorLoc	86.2 \pm 1.7	89.3 \pm 1.5	91.4 \pm 1.5
Health advice	89.4 \pm 1.5	92.1 \pm 1.8	94.2 \pm 1.7
Forest cover	90.3 \pm 1.4	91.2 \pm 1.4	94.3 \pm 1.3
Gene expression	88.3 \pm 1.4	90.2 \pm 1.3	93.3 \pm 1.5

likely to end up flipping to another cancer type.

E. Local interpretability

First, we randomly pick a sample from the test set. Assuming XGBoost predicts the instance is of *COAD* cancer type, the contribution plot (fig. 7 in supplementary) outlines how much contribution individual features had on this prediction. Features (genes) DNMT3A, SLC22A18, RB1, CDKN18, MYB are top-k features w.r.t impact values, while features CASP8 and MAP2K4 had negative contributions. Further, to quantitatively validate the impact of top-k features and to assess feature-level relevances, we carry out *what-if* analysis. As shown, the observation is of *COAD* with a probability of 55% and *BRCA* type with a probability of 29%. Features on the right side (i.e., TFAP2A, VPS9D1-AS1, MTND2P28, ADCY3, and FOXP4 are positive for *COAD* class, where feature TFAP2A has the highest positive impact of 0.29) positively impact the prediction, while features on the left negatively. Genes TFAP2A, VPS9D1-AS1, MTND2P28, ADCY3, FOXP4, GPRIN1, EFNB1, FABP4, MGP, AC020916-1, CDC7, CHADL, RPL10P6, OASL, and PRSS16 are most sensitive to making changes, while features SEMA4C, CWH43, HAGLROS, SEMA3E, and IVL are less sensitive to making changes.

If we remove feature TFAP2A from the profile, we would expect the model to predict the observation of *COAD* cancer type with a probability of 26% (i.e., 55% - 29%). This will recourse the actual prediction to *BRCA* in which features IVL, PRSS16, EFNB1, and CWH43 are most important, having impacts of 0.23, 0.17, 0.123, and 0.07, respectively. These

features not only reveal their relevance for this decision but also signify that removing them is like to impact the final prediction. Further, we focus on local explanations for this prediction by connecting *decision rules* and counterfactuals with additive feature attributions (AFA) in fig. 8. While Anchor provides a single rule outlining which features impacted at arriving this decision, LIME generates AFA stating which features had positive and negative impacts. However, using decision rules and a set of counterfactuals, we show how the classifier could arrive at the same decision in multiple ways due to different negative or positive feature impacts.

V. CONCLUSION

In this paper, we proposed an efficient technique to improve the interpretability of complex black-box models trained on high-dimensional datasets. Our model surrogation strategy is equivalent to the knowledge distillation process for creating a simpler model. However, instead of training the *student* model on *teacher's* predictions, we transferred learned knowledge (e.g., top-k or globally most and least important features) to a student and optimize an objective function. Further, the more trainable parameters are in a black-box model, the bigger the size of a model would be. This makes the deployment infeasible for such a large model in resource-constrained devices¹⁵. Further, the inferencing time of large models increases and ends up with poor response times due to network latency even when deployed in a cloud infrastructure, which is unacceptable in many real-time applications. We hope our model surrogation strategy would help create simpler and lighter models and improve interpretability in such a situation.

Depending on the complexity of the modelling tasks, a surrogate model may not be able to fully capture a complex black-box model. Consequently, it may lead users to recommend wrong conclusions (e.g., in healthcare) - especially if the knowledge distillation process is not properly evaluated and validated. In the future, we want to focus on other model

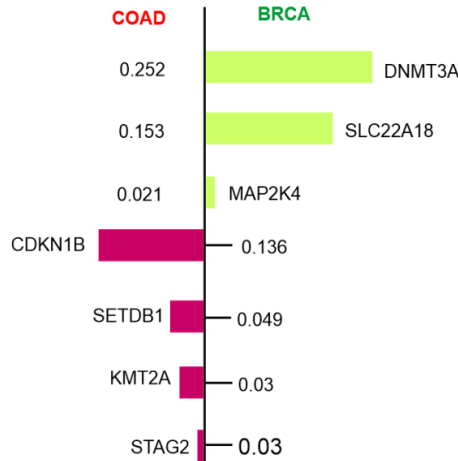
¹⁵ e.g., IoT devices having limited memory and low computing power.

LORE:

$$r = \{MAP2K4 \geq 8.23, EZH2 \geq 2.92, DNMT3A \geq 0.63, KMT2A < 0.77, CDKN1B < 0.47 \rightarrow decision = BRCA\}$$

$$\Phi = \{ \{DNMT3A \geq 0.63, KMT2A < 0.77, CDKN1B \leq 1.41, PTEN > 2.70, STAG2 > 2.24 \rightarrow decision = COAD\}, \\ \{MYB \leq 1.08, KMT2C > 0.64, RUNX1 \leq 6.38, SLC22A18 \leq 6.43, PTEN > 2.70 \rightarrow decision = COAD\}, \\ \{RUNX1 \leq 6.38, MYB > 0.058, FOXA1 \leq 3.35, KMT2A \leq 0.81, RB1 \leq 3.34 \rightarrow decision = COAD\} \}$$

LIME:



Anchor:

$$r = (\{CDKN1B < 0.47, SETDB1 < 0.70, STAG2 < 3.29, PTEN > 2.70, CASP8 \leq 0.58\} \rightarrow decision = BRCA)$$

Fig. 8: Example of explaining single prediction using rules, counterfactuals, and additive feature attributions

compression techniques such as quantization (i.e., reducing numerical precision of model parameters or weights) and pruning (e.g., removing less important parameters or weights).

ACKNOWLEDGEMENT

This paper is a collaborative effort and based on the PhD thesis [17] by the first author and the second author's work as part of the *Marie Skłodowska-Curie* project funded by the *Horizon Europe 2020* research and innovation program of the *European Union* under the grant agreement no. 955422.

REFERENCES

- [1] Q. Fournier and D. Aloise, "Empirical comparison between autoencoders and traditional dimensionality reduction methods," in *2019 IEEE Second International Conference on Artificial Intelligence and Knowledge Engineering (AIKE)*. IEEE, 2019, pp. 211–214.
- [2] C. C. Aggarwal and C. K. Reddy, *Data clustering: algorithms and applications*. CRC press, 2014.
- [3] M. R. Karim, T. Islam, M. Cochez, D. Rebholz-Schuhmann, and S. Decker, "Explainable AI for Bioinformatics: Methods, Tools, and Applications," *Briefings in Bioinformatics*, 2023.
- [4] M. E. Kaminski, "The right to explanation, explained," *Berkeley Tech. LJ*, vol. 34, p. 189, 2019.
- [5] S. Wachter, B. Mittelstadt, and C. Russell, "Counterfactual explanations without opening the black box: Automated decisions and the GDPR," *Harv. JL & Tech.*, vol. 31, p. 841, 2017.
- [6] C. Molnar, *Interpretable machine learning*. Lulu.com, 2020.
- [7] M. Ribeiro, S. Singh, and C. Guestrin, "Local interpretable model-agnostic explanations (LIME): An introduction," 2019.
- [8] H. Lakkaraju, E. Kamar, R. Caruana, and J. Leskovec, "Faithful and customizable explanations of black box models," in *Proceedings of AAAI/ACM Conference on AI, Ethics, and Society*, 2019, pp. 131–138.
- [9] S. M. Lundberg and S.-I. Lee, "A unified approach to interpreting model predictions," in *Advances in neural information processing systems*, 2017, pp. 4765–4774.
- [10] T. Miller, "Explanation in artificial intelligence: Insights from the social sciences," *Artificial Intelligence*, 2018.
- [11] A. Chattopadhyay and A. Sarkar, "Grad-CAM++: Generalized gradient-based visual explanations for deep convolutional networks," in *Conf. on Applications of Computer Vision (WACV)*. IEEE, 2018, pp. 839–847.
- [12] S. Bach, A. Binder, G. Montavon, K.-R. Müller, and W. Samek, "On pixel-wise explanations for non-linear classifier decisions by layer-wise relevance propagation," *PloS one*, vol. 10, no. 7, 2015.
- [13] B. Škrlj, S. Džeroski, N. Lavrač, and M. Petkovič, "Feature importance estimation with self-attention networks," *arXiv preprint arXiv:2002.04464*, 2020.
- [14] S. O. Arık and T. Pfister, "TabNet: Attentive interpretable tabular learning," in *AAAI*, vol. 35, 2021, pp. 6679–6687.
- [15] M. T. Ribeiro, S. Singh, and C. Guestrin, "Anchors: High-precision model-agnostic explanations," in *Thirty-Second AAAI Conference on Artificial Intelligence*, 2018.
- [16] R. Guidotti, A. Monreale, S. Ruggieri, D. Pedreschi, F. Turini, and F. Giannotti, "Local rule-based explanations of black box decision systems," *arXiv preprint arXiv:1805.10820*, 2018.
- [17] M. R. Karim, D. Rebholz-Schuhmann, and S. Decker, "Interpreting black-box machine learning models with decision rules and knowledge graph reasoning," Aachen, Germany, June 2022. [Online]. Available: <https://publications.rwth-aachen.de/record/850613>
- [18] M. D. Zeiler, G. W. Taylor, and R. Fergus, "Adaptive deconvolutional networks for mid and high level feature learning," in *2011 international conference on computer vision*. IEEE, 2011, pp. 2018–2025.
- [19] A. Vaswani, N. Shazeer, N. Parmar, J. Uszkoreit, L. Jones, A. N. Gomez, L. Kaiser, and I. Polosukhin, "Attention is all you need," *Advances in neural information processing systems*, vol. 30, pp. 5998–6008, 2017.
- [20] S. M. Lundberg and S.-I. Lee, "Consistent feature attribution for tree ensembles," *arXiv preprint arXiv:1706.06060*, 2017.
- [21] R. M. Grath, L. Costabello, C. L. Van, P. Sweeney, F. Kamiab, Z. Shen, and F. Lecue, "Interpretable credit application predictions with counterfactual explanations," *arXiv preprint arXiv:1811.05245*, 2018.
- [22] J. Torres-Sospedra, R. Montoliu, A. Martínez-Usó, T. J. Arnau, M. Benedito-Bordonau, and J. Huerta, "Ujiindoorloc: A new multi-building and multi-floor database for wlan fingerprint-based indoor localization problems," in *2014 international conference on indoor positioning and indoor navigation (IPIN)*. IEEE, 2014, pp. 261–270.
- [23] J. A. Blackard and D. J. Dean, "Comparative accuracies of artificial neural networks and discriminant analysis in predicting forest cover types from cartographic variables," *Computers and electronics in agriculture*, vol. 24, no. 3, pp. 131–151, 1999.